BEAM DYNAMICS SIMULATION IN SARAF PHASE-I PROTON/DEUTERON 4 MEV LINAC COMMISSIONING

J. Rodnizki, A. Kreisel, Soreq NRC, Yavne 81800, Israel

Abstract

The SARAF accelerator is designed to accelerate both deuteron and proton beams up to 40 MeV. Phase I of SARAF consists of a 4-rod RFQ (1.5 MeV/u) and a prototype superconducting module housing 6 half-wave resonators (HWR) and 3 superconducting solenoids (4-5 MeV). Beam Dynamics TRACK simulation, for a proton and a deuteron beam, tailored to the present available field amplitude at each cavity, were used to evaluate and tune the linac. The simulation is a key factor to reach a stable high intensity CW beam. The ions energy and energy spread were measured using the Rutherford scattering technique. The measured energy gain and the energy spread at the RFQ exit and along the PSM were in good agreement with the beam dynamics simulations.

INTRODUCTION

SARAF (Soreq Applied Research Accelerator Facility) is currently under construction at Soreq NRC. It will consist of up to 40 MeV high current (up to 4 mA) CW, 176 MHz RF superconducting linac of protons and deuterons. The linac status and technical description of its components are given in [1]. Phase one of the SARAF linac includes a 20 keV/u proton/deuteron ECR ion source, a LEBT, a 3.8 m long 1.5 MeV/u four rods RFQ and a Prototype Superconducting Module (PSM) with six $\beta = 0.09$ HWRs, a Diagnostic plate (D-plate), Beam Dumps (BD) and a temporary beam line . The main components of Phase I are shown in Fig. 1.

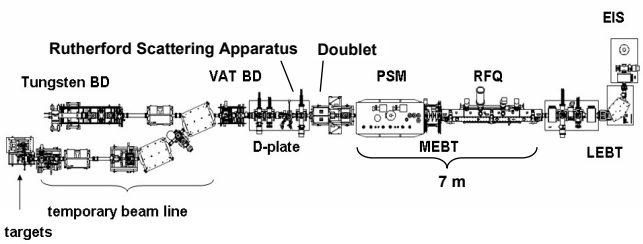

Figure 1: Phase I of the SARAF linac.

Beam dynamics simulations were vital during the conditioning efforts of phase I. At each step of the operation the low level RF amplitude and phase were varied to achieve the beam dynamics design. The electromagnetic fields were simulated using CST MWS and the presented beam dynamics simulations were done using TRACK [2].

The simulations were applied for:

1. Analysis of the RFQ beam transmission as function of the RFQ power.
2. Optimization of the RFQ field flatness to achieve better transmission and lower losses downstream the RFQ.
3. Exploring and calibrating the voltage at each cavity as a function of the low level RF signal.
4. Beam dynamics design of the fields configuration according to the achievable measured voltage in each cavity.

ANALYSIS OF RFQ BEAM OPERATION

A comparison of proton beam dynamics simulation to a measurement in 2007 is presented in Fig. 2 top. It shows good agreement at the low power region and a reduction in the measured transmitted current in the high power region relative to the simulated value [3]. The expected value was extracted from beam dynamics simulations with homogenous fields along the RFQ.

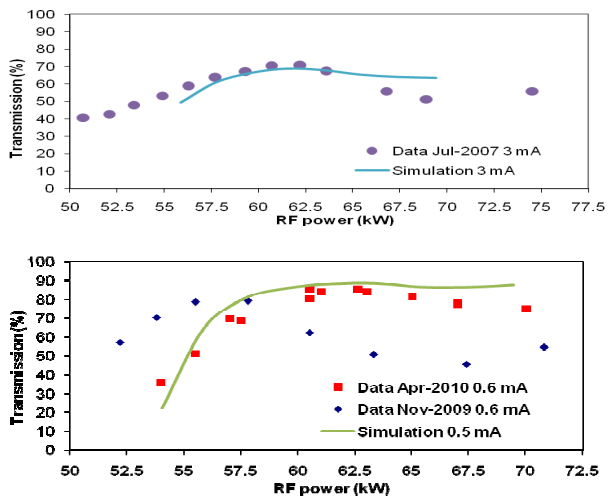

Figure 2: Proton transmitted current as function of RFQ power. Comparison of data and simulation for high current 3mA (top) and low current ~0.5 mA (bottom).

Prior to 2009 measurements the bottom electrodes were re machined due to high parasitic fields that eliminated CW deuteron beam operation. The quadrupole electrodes design, so called 'mini-vane', has a cooling water channel drilled inside. The mini-vanes allow a good cooling of the electrodes and avoids misalignment caused by heating. In the SARAF RFQ mini-vanes design the distance between the bottom electrodes and the stems with the negative RF polarity (each second stem) was too small (around 5 mm). This resulted in parasitic fields between the bottom electrodes and the stems, which are higher than the fields between the electrodes, as proved by RF simulations.

To solve this problem local cutting of the bottom electrodes back side along each second stem reduced

significantly these parasitic fields and allowed to doubl the RFQ operational power, see Fig. 3.

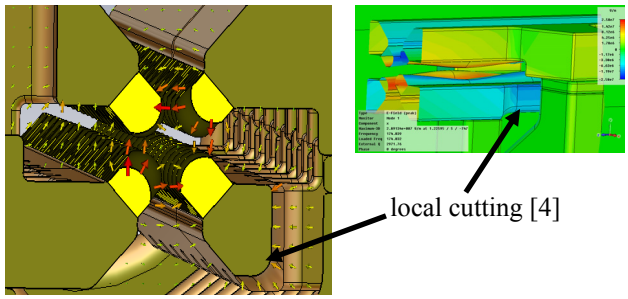

Figure 3: The reduced parasitic fields at the back of the bottom electrodes due to local cutting.

The RFQ resonance frequency was increased since the electrodes capacitance was reduced. The tuning plates along the high modulation section with lower capacity per unit length, were removed, the horizontal distance between the electrodes at the last section was reduced by 400 μm, which partially compensated for the reduction in capacity. The field profile was measured and reproduced by CST MWS eigen mode simulation, see Fig. 4.

An unwanted outcome of the re machining was a distortion in the field flatness at the last section of the RFQ as seen in Fig. 4 for 2009. Misalignments and inhomogeneous fields along the RFQ can result in a reduction in transmission as function of power. This was tested in Nov-2009 by measuring the RFQ transmission as function of the RFQ power. The measurements revealed a further reduction in the RFQ transmission, at the high power range as shown in Fig. 2 bottom.

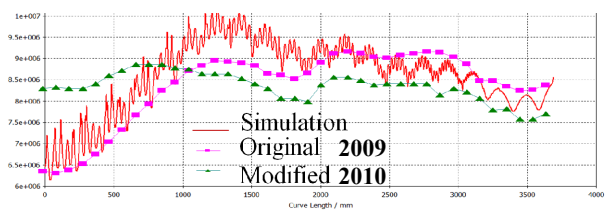

Figure 4: The original, simulated and modified field flatness along the RFQ. Beam direction is right to left.

A beam dynamics analysis was conducted to explore the effect of the distorted field homogeneity in the last section of the RFQ. The simulated input voltage of the 190 modulated cells was taken from the original 2009 measured one (Fig. 4). The effect of beam loss due to the distorted field was then studied as function of the RFQ voltage for 500k simulated macro particles, see Fig. 5. The simulations present losses at the RFQ exit section for the distorted field configuration.

From looking at the phase space diagrams extracted from the distorted field configurations (top & middle) it could be deduced that the losses at the RFQ exit are transverse losses (Fig. 6).

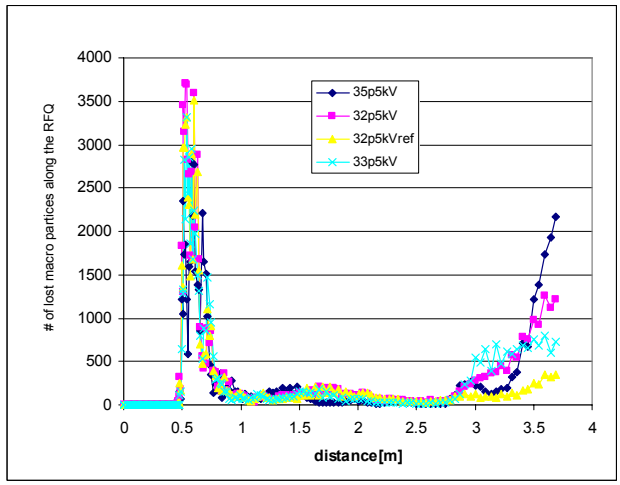

Figure 5: Macro particles lost along the RFQ, Each macro-particle = 8 nA. The lost are presented for different electrode average voltages [35.5, 33.5, 32.5] kV with the measured distorted field, and with the nominal homogenous field 32.5 kV (yellow triangle).

The envelope of the transversal phase spaces for the distorted field configurations are larger than the flat field one. This is also confirmed in the transversal beam profiles measured at the MEBT (Fig. 7 left). These transversal losses at high beam current increase the vacuum pressure at the PSM preventing transmission of high intensity beam through the PSM [1].

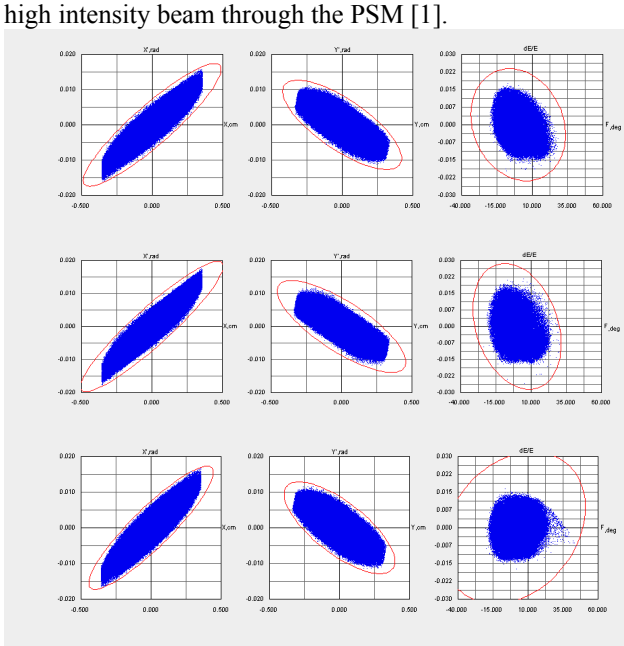

Figure 6: Phase space at the RFQ exit for the 2009 field profile: 32.5 kV tuned field (top), 35.5 kV tuned field (middle), and for the 32.5 kV reference "homogenous" field design (bottom).

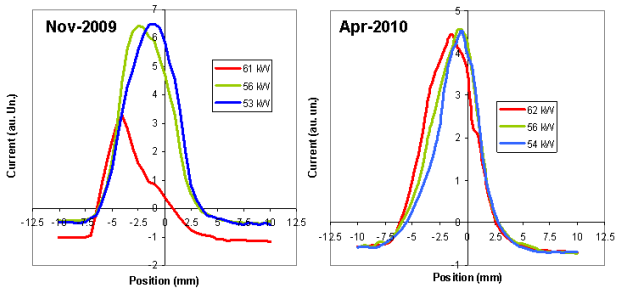

Figure 7: Beam profile measurements at the MEBT before and after shims replacement and field flattening.

The beam dynamics study point out that the transversal losses at the RFQ exit and the reduction in the RFQ transmission could have been originated by the field distortion at the RFQ. The solution was to reduce the vertical distance between the electrodes at the last section of the RFQ in order to achieve field flatness. The distance between the electrodes was reduced by replacing the existing shims at the last section with longer shims at the bottom electrodes and shorter shims at the top electrodes, see Fig. 8.

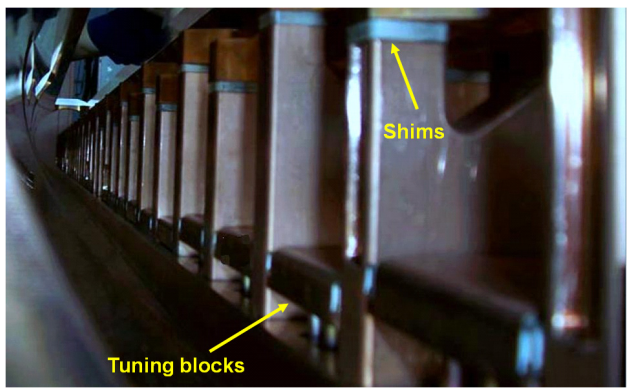

Figure 8: A RFQ picture showing the electrodes contact to the supported stems by shims.

CST MWS simulation sensitivity study suggested that enlarging the length of the bottom electrodes by 300 μm and reducing the length of the top electrode by 300 μm at the last section will enable insertion of an additional tuning plate at the last section. Following the CST MWS study, the shims were replaced. The actual vertical distance between the rods was reduced by 400 μm and in addition the rods moved horizontally closer to each other by another 200 μm. The field flatness is now maintained along the RFQ including the last section (Fig. 4, modified 2010). The modification resulted in elimination of the reduction in the RFQ transmission at high power (Fig. 2 bottom, April 2010). This behavior is in good agreement with the beam dynamics prediction for the expected transmission as function of RFQ power as seen in this figure. In addition the beam profile became narrower (Fig. 7 right) as predicted in the simulations (Figs. 5 and 6). After correcting the RFQ field inhomogeneous and retune the MEBT quadrupoles as extracted from the TRACK simulations, we were manage to transmit and accelerate a 1 mA CW 3.1 MeV stable proton beam through the PSM with moderated pressure increase in the PSM [1].

ANALYSIS OF PSM BEAM OPERATION

Cavities Tune

Beam dynamics simulations using the TRACK code established the design of the PSM operation setup. Beam particle energy and energy spread were measured using Time of Flight (TOF) and Rutherford Scattering (RS) techniques, in order to calibrate the cavities to the desired setup [5, 6]. In the analysis of the PSM operation the RS apparatus was used for phasing of individual cavities. The RS apparatus is constructed from a 0.15 μm gold foil which is inserted to the beam halo zone and a silicon detector at angle of 45 degrees. The ions energy and bunch energy spread as a function of the first cavity (HWR1) phase are shown in Fig. 9. For this measurement the other five cavities were turned off and detuned. The dependence of the energy and energy spread on the cavity accelerating phase is clearly seen in Fig. 9. The energy values determined by the two methods are consistent. While TOF measures only the mean energy of the bunch, the RS measures the bunch energy spectrum, and allows studding bunching effects of the resonators.

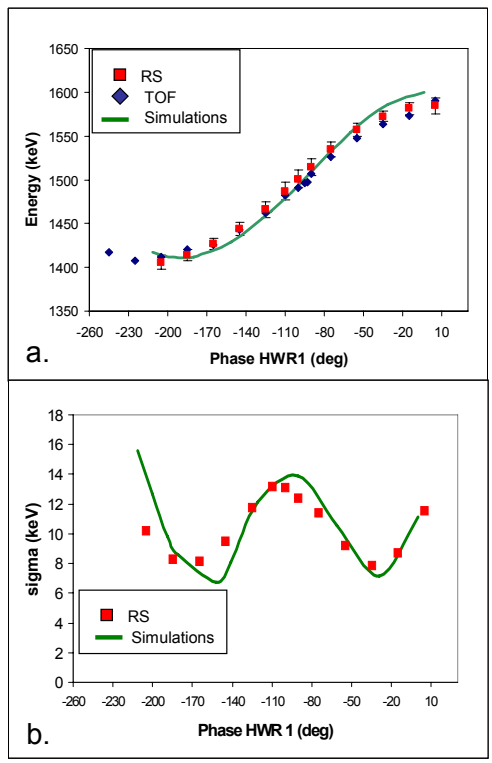

Figure 9: Proton beam energy (a) and the energy spread width (b) as a function of HWR1 phase, as determined by TOF and RS and compared to TRACK simulations.

The operational voltage and the synchronous phase of the resonators were determined cavity by cavity starting with the first upstream resonator and keeping the downstream ones detuned and turned off. The bunch energy gain as a function of phase (Fig. 10) was

compared with simulation allowing one to calibrate the resonator voltage. The real voltage and the synchronous phase were reached iteratively during pulse 1 Hz, 100 μs, a 0.24 mA beam operation, based on beam dynamics analysis as shown in Fig. 10. Beam dynamics parameters, including the applied Low Level RF (LLRF) values, to reach the design of a 3.1 MeV, 2 mA, proton beam are given in Table 1. The first step is to calibrate the cavity LLRF set voltage to the realistic voltage. The calibration is based on the simulated beam energy gain through the cavity as function of the input cavity voltage (Fig. 11). The next step is to set the phase that will match the synchronous phase for the set calibrated cavity voltage. The tune of the cavities started with the first cavity which is operated as a buncher, 1 m downstream the RFQ exit. The second cavity is detuned to enable gentle converging of the beam prior to beam acceleration which starts with the third cavity. The tune was done with an effort to minimize the longitudinal emittance growth based on the available HWRs cavity voltage.

Table 1: Beam Dynamic Design and Matched LLRF Values

HWR	Set V kV	Real V kV	Set Phase Deg.	Sync. Phase Deg.
1	154	150	20	-95
2	Off			
3	560	500	-60	0
4	400	500	105	-35
5	550	500	255	-30
6	520	500	0	0

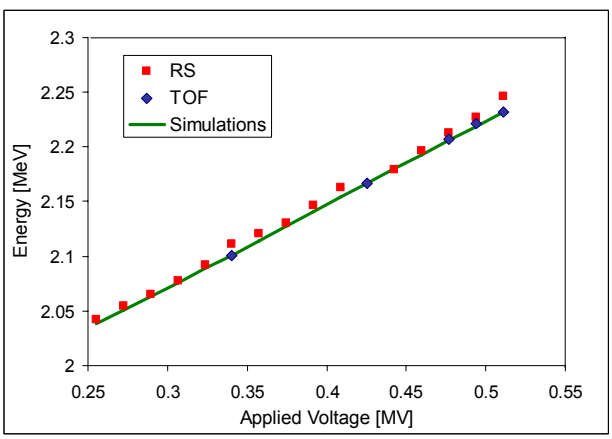

Figure 11: Proton energy as a function of HWR4 voltage, while the three previous resonators were also operated.

Longitudinal Emittance Construction

An algorithm was derived to evaluate the beam longitudinal emittance based on the measured beam energy spread using the RS method. It was shown [5] that the longitudinal emittance along the PSM, denoted as σ_e, could be reconstructed by measuring the energy spread

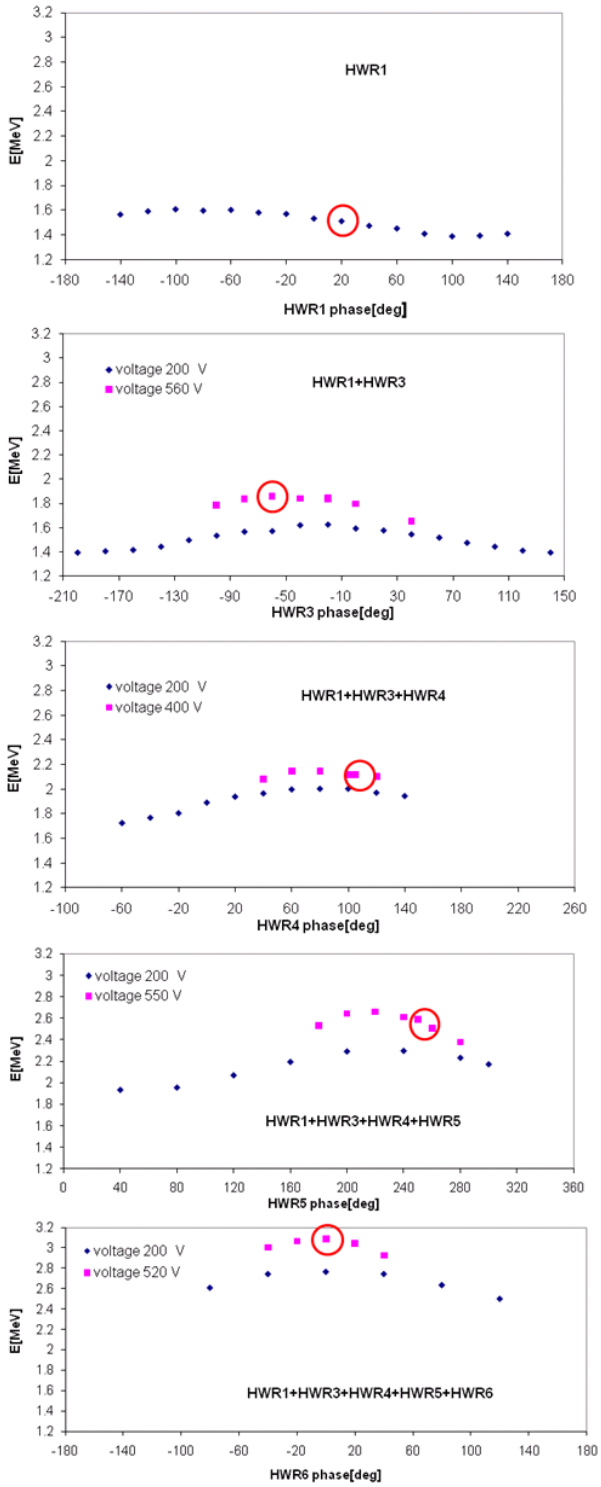

Figure 10: Protons energy as a function of the tuned cavity set phase, while the upstream cavities were locked and the downstream cavities were detuned and turned off.

variance at the RS apparatus, denoted as σ_{66x}.The variance of the energy spread measured as a function of the last cavity energy gain per degree, denoted as X, is a quadratic polynomial, see Figs. 12 and 13. The polynomial function parameters are related to the reconstructed emittance matrix elements, σ_e:

$$\sigma_{66x}(X) = (\sigma_{55e} + 2Y\sigma_{56e} + Y^2\sigma_{66e})X^2 + 2(\sigma_{56e} + Y\sigma_{66e})X + \sigma_{66e} = p_1X^2 + p_2X + p_3$$

$$\sigma = \varepsilon\begin{bmatrix}\hat{\beta} & -\hat{\alpha}\\ -\hat{\alpha} & \hat{\gamma}\end{bmatrix} = \begin{bmatrix}\sigma_{55} & \sigma_{56}\\ \sigma_{65} & \sigma_{66}\end{bmatrix}$$

$$Y = -\left((360/T)*(D/\beta c)\right)/(mc^2\gamma^3\beta^2)$$

where T is the beam period ($T=1/f$, $f=176$ MHz), m is the particle mass and D is the drift distance between the extracted point along the PSM and the diagnostic cavity.

This algorithm was adopted for the emittance measurements of a proton beam. The measurements were taken with the same configuration as in table 1 with the following differences, cavity 3 voltage was 590 kV, Cavity 5 was detuned and the diagnostic cavity, cavity 6, was operated as a buncher at -95 degrees synchronous phase. The energy variance at the halo monitor was measured as a function of cavity 6 acceleration voltage from 53-530 keV. The outcome of the polynomial fit, see Figs. 12 and 13, gives a deconstructed rms longitudinal emittance value of 90±5 πdeg-keV, at the exit of cavity 4, for a 0.24 mA proton beam. This value is larger from the beam dynamics simulation value of 60 πdeg-keV. The measured energy spread at the RS apparatus is a convolution of the beam energy spread and the intrinsic resolution of the RS measurement. An evaluation of the RS measurement resolution was conducted. There are two main contributions, one from the variance of the energy loss in the gold foil, and the second is due to the resolution in the silicon detector. The average energy loss in the gold foil is 18 keV. The contributing factors to the variance of the energy loss in the gold foil are: The struggling energy for a 1.5 MeV proton beam based on [7] is $(3.6\ \text{keV})^2$. The variance in the energy loss due to the various path length is $(1.7\ \text{keV})^2$. The corresponding values from TRIM simulations are $(5\ \text{keV})^2$ and $(2\ \text{keV})^2$. The geometric variance due to the horizontal position of the proton projectile along the gold foil (as function of the scattering angle) is negligible $(0.3\text{keV})^2$. The silicon detector contributions are: the struggling energy through the dead layer, the variance of the energy spent on crystal damage and lattice vibration, the variance in the number of created electron hole pairs, and the statistical distribution of the energy due to electronics resolution. The total quote FWHM range of a silicon PIPS detector, for a 1.5-3 MeV proton projectile is [10- 12 keV]. The resulted silicon detector variance range is $(4.25\ \text{keV})^2$-$(5.1\ \text{keV})^2$. Summing all the variance contributions gives $(5.8\ \text{keV})^2$– $(7.4\ \text{keV})^2$. The good agreement between the simulated and measured energy spread width (Fig. 9) indicates that the lower estimated value for the intrinsic variance of the RS apparatus is more probable. For longitudinal emittance construction, the contribution of the RS apparatus intrinsic variance was not extracted from the measured beam energy variance. The longitudinal emittance was similarly reconstructed for a deuteron beam.

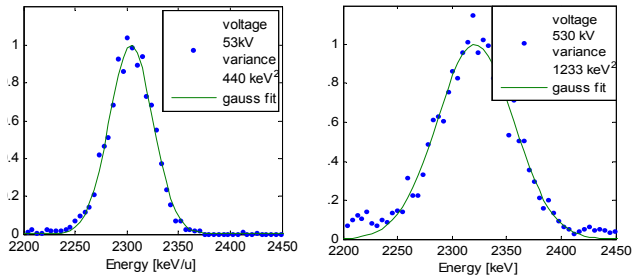

Figure 12: The proton beam measured energy distribution for different cavity applied voltages.

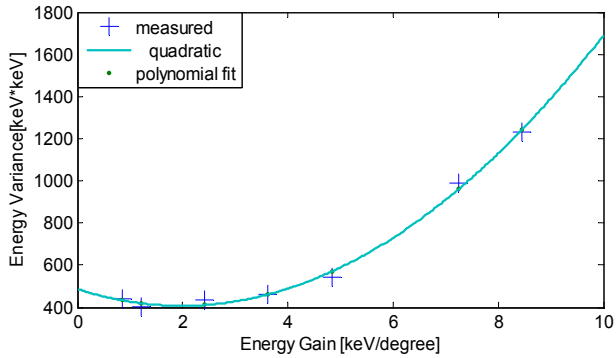

Figure 13: The proton beam measured energy variance versus the energy gain per degree in the diagnostic cavity.

The minimal measured emittance at the RFQ exit was applied to select the RFQ power for acceleration of a 2.17 MeV/u, 0.4 mA deuteron beam at low duty cycle using the PSM based on beam dynamics simulation [5].

CONCLUSION

Beam dynamics simulations accompanied by beam diagnostics had a vital contribution to achieve a stable CW proton beam at the SARAF phase I linac.

REFERENCES

[1] L. Weissman et al., "SARAF Accelerator Commissioning Results", LINAC'10, Tsukuba, Sept. 2010, WE102.
[2] P. N. Ostroumov et al., "TRACK", ANL, March 2006.
[3] C. Piel et al., "Phase 1 Commissioning Status of the 40 MeV Proton/Deuteron Accelerator SARAF", EPAC'08, Genoa, June 2008, THPP038 (2008).
[4] I. Mardor et al., "The Status of the SARAF CW 40 MeV Proton/Deuteron Accelerator", PAC'09, Vancouver, May 2009, FR5REP087 (2009).
[5] J. Rodnizki et al., "Energy and energy spread measurements using the Rutherford scattering technique for tuning the SARAF superconducting linac", LINAC'10, Tsukuba, Sept. 2010, TUP091.
[6] L. Weisman et al., "First Experience with Proton Beams Using the Rutherford Scattering Monitor", DIPAC09, Basel (2009).
[7] W. K. Chu, Physical Review A 13(6) (1976) 2057-2060.